Linear Rheology of Architecturally Complex Macromolecules: Comb Polymers with Linear Backbones

M. Kapnistos,[†,‡] D. Vlassopoulos,[*,†,§] J. Roovers,[⊥] and L. G. Leal[‡]

Institute of Electronic Structure & Laser, Foundation for Research and Technology−Hellas (FORTH), Heraklion 71110, Crete, Greece; Department of Chemical Engineering, University of California at Santa Barbara, Santa Barbara, California 93106; Department of Materials Science & Technology, University of Crete, Heraklion 71003, Crete, Greece; Institute for Chemical Process and Environmental Technology, National Research Council, Ottawa, Ontario K1A OR6, Canada

Received March 28, 2005; Revised Manuscript Received May 26, 2005

ABSTRACT: We present a detailed, systematic study of the linear rheological response of model comb homopolymers consisting of linear backbone chains on which branches of the same polymer are grafted. By using polymers of different molecular weights of backbone and branches, different number of branches, and different chemistries, we explore the relaxation mechanisms of these polymers and find their universal features. We apply a tube model theoretical analysis, originally developed by McLeish and co-workers, which has been appropriately modified in order to account for the effects of the fluctuations of the free ends of the backbone (due to the grafting procedure during synthesis) and the polydispersity on the rheology. The satisfactory fitting of the data with the model indicates that the latter is capable of providing a quantitative understanding of the rheology of branched polymers. More specifically, comb polymers exhibit two distinct relaxation processes, assigned to the branches and the backbone. Relaxation proceeds hierarchically with the grafted branches moving first. The free backbone ends contribute as extra asymmetric branches moving via fluctuations. Finally, important issues relating to the number of grafted branches and the possible tube dilation breakdown (which may explain the physics of the only adjustable parameter p^2) are discussed.

I. Introduction

It is well-known that controlling the rheology of entangled polymers represents the key for understanding, and thus monitoring, their processing performance and final product properties. It is also widely accepted that the tremendous progress made to date is almost exclusively based on two factors: the unparalleled impact and success of the tube model for the entanglements and the anionic synthesis of well-characterized model polymers.[1−7] With the field of linear polymer rheology mature,[8] attention has shifted to branched polymers for two main reasons: (i) it is natural question of fundamental interest to explore the effects of topological complexity on the rheology and in particular the possible combination of reptative and nonreptative modes of motion; (ii) nearly all commercial polymers (e.g., polyethylene) and systems of biological interest (e.g., self-assemblies within the cell) consist of branched structures.[9,10]

Star polymers, the simplest branched polymers, relaxing exclusively via branch fluctuations, are reasonably well understood.[11,12] This is due to the seminal recent work of Milner and McLeish,[12,13] who combined a tube model with the idea of dynamic tube dilution (DTD: relaxed segments act as solvents to the rest of the molecule, thus effectively increasing the tube diameter) to describe the relaxation of star polymer melts. That work in a sense has revolutionized a seemingly stagnant field, as it lead to many bright ideas for improvements (all of which however converge to the success of the tube model but raise reasonable questions with respect to the extent of validity of the DTD picture), and more importantly, it opened the route for investigating more complex topologies such as H-polymers,[14] comb polymers,[15] and more structured dendritically branched polymers,[16] within the DTD framework. The key concept here is the hierarchy of motions.[17] In other words, entanglements belonging to topologically different parts of the macromolecule (branches or backbone or different layers) relax in a certain sequence, obeying seniority rules according to which the outer parts of the molecule relax first and the inner ones last; only when the last relaxation has been completed the whole molecule has relaxed.

In this paper, we present a systematic investigation of the linear rheology of comb polymers with linear backbones. We demonstrate that these polymers indeed relax hierarchically and show that the tube models for combs, appropriately extended to account for the macromolecular structures at hand, are successful in describing the response of these systems. We use model polymers of different (a) chemistry (polybutadienes of predominantly 1,4-addition, polystyrenes), molecular weights of (b) backbone, and (c) grafted branches and (d) number of grafted branches, as discussed in section II. The experimental procedure and features of the systems studied are presented in section III. Section IV presents the full tube model with the added extensions and corrections, whereas the comparison of theory and data is presented in section V, where remaining problems (associated with the friction of the branching points and the number of branches) are discussed and possible remedies are outlined. The key conclusions are summarized in section VI.

II. Experimental Section

Materials. Linear comb polymers consisting of a linear backbone on which linear chains (called branches) are chemi-

[†] Foundation for Research and Technology−Hellas (FORTH).
[‡] University of California at Santa Barbara.
[§] University of Crete.
[⊥] National Research Council.

10.1021/ma050644x CCC: $30.25
Published on Web 07/30/2005

Table 1. Molecular Characteristics of the Samples Used

sample	M_b (kg/mol) backbone	M_a (kg/mol) branch	q (branches/ backbone)[a]	M_{total} (kg/mol)
lc1-PBd[b]	50	11.3	18	256
lc2-PBd	50	23.2	17.8	464
lc3-PBd	50	7	17	177
c6bb-PS[c]	275			275
c612-PS	275	6.5	31	475
c622-PS	275	11.7	30	624
c632-PS	275	25.7	25	913
c642-PS	275	47	29	1630
c652-PS	275	98	29	3130
c7bb-PS	860			860
c712-PS	860	6.5	30	1055
c722-PS	860	11.7	28	1190
c732-PS	860	25.7	26	1530
c742-PS	860	47	29	2530
c752-PS	860	98	28	3620

[a] Note that there is a slight uncertainty in the determination of variance in the number of branches, as explained in ref 19. [b] PBd samples from ref 19. [c] PS samples from ref 18.

cally grafted, of different chemistry (polystryrene, PS, and 1,4-polybutadiene, PBd), were synthesized anionically and carefully characterized in the past.[18,19] The PS comb series c6 and c7 consist of a linear backbone with weight-average molecular weight M_b = 275 000 and 860 000 g/mol, respectively, and approximately $q = 25-30$ linear branches of varying molecular weight M_a from 6500 to 98 000 g/mol,[17] i.e., from unentangled to well-entangled (for PS a typical literature value of the entanglement molecular weight is M_e = 17 000 g/mol).[20,21] The PBd linear combs consist of linear backbone (50 000 g/mol) and 17−18 grafted linear branches of various sizes (from 7000 to 23 200 g/mol),[19] all entangled (for PBd a typical literature value of the entanglement molecular weight is M_e = 1815 g/mol)[20,21] and stored in vacuum-sealed glass tubes at −20 °C before use. Table 1 lists the main molecular characteristics of all samples used in this work. As the condition of the samples can be a concern, the unchanged value of the plateau modulus (discussed below) with respect to refs 18 and 19, as well as standard literature data in ref 21, signals their pristine shape. In particular, for the PBd samples (which are more susceptible to degradation and aging), a more sensitive way to check their condition is via the zero-shear recoverable compliance (J_e^0). The values of J_e^0 (in Pa^{-1}) for samples lc1-PBd, lc2-PBd, and lc3-PBd from recent (this work) and old (ref 19) measurements are respectively 5.9×10^{-5}, 14.1×10^{-5}, 3.9×10^{-5} and 5.7×10^{-5}, 11×10^{-5}, 3.5×10^{-5}, referring to the same temperature (27 °C). This confirms that the samples are intact.

Rheology. The measurements were conducted on a Rheometric Scientific strain-controlled rheometer (ARES 2KFRTN1) in the parallel plate geometry, with a temperature control of ±0.1 °C (achieved via an air/nitrogen convection oven and a liquid nitrogen Dewar), under nitrogen environment to reduce the risk of degradation (testing the reproducibility of the measurements served as the check of sample condition). Before measurements, the samples were press-molded under vacuum into diskotic specimens with diameter 8 mm and height 1−1.5 mm. Dynamic rheological measurements were carried out in the temperature range −90 to 100 °C for PBd samples and 120 to 210 °C for PS samples. Dynamic time sweep and strain sweep experiments were conducted to ensure thermal equilibrium of the sample and determine the linear viscoelastic region for the frequency sweeps (small-amplitude oscillatory shear). The time−temperature superposition principle was used in order to combine frequency sweep experiments at different temperatures and create the master frequency spectrum (Figures 1 and 2). The data were first vertically shifted by a vertical shift factor, which was determined from the change of density with temperature: $b_T = \rho(T_{ref})(T_{ref} + 273.15)/\rho(T)(T + 275.15)$; T is in °C. This shift factor was common for all data of the same chemistry. Note that the used temperature dependencies of the densities (in g/cm^3) for PS and PBd are given by $\rho(T) = 1.2503 - 6.05 \times 10^{-4}(273.15 + T)$ and $\rho(T) = 1.0547 - 5.6 \times 10^{-4}(273.15 + T)$, respectively.[22] Subsequently, the data were shifted along the frequency axis, and the horizontal shift factors for all PBd samples were fitted with a single set of parameters of the WLF function:[21] $\log a_T = [-C_1(T - T_{ref})]/[C_2 + T - T_{ref}]$ with T_{ref} = 0 °C, $C_1 = 4.9$, and C_2 = 154 °C (Figure 3a). Similarly, the PS samples have T_{ref} = 170 °C, $C_1 = 5.6$, and C_2 = 120 °C (Figure 3b).

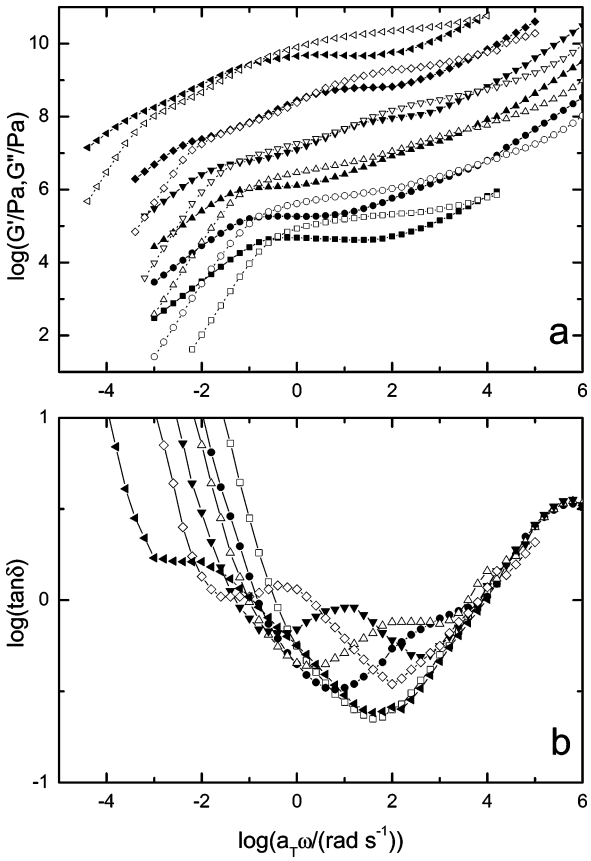

Figure 1. Linear rheology of PS linear combs with equal backbone (M_b = 275 kg/mol) and increasing branch lengths. (a) The dynamic moduli and (b) the tangent of the phase angle: (■, □, and −□−) c6bb-PS, (●, ○, and −●−) c612-PS, (▲, △, and −△−) c622-PS, (▼, ▽, and −▼−) c632-PS, (◆, ◇, and −◇−) c642-PS, (tilted ▲, △, and −▲−) c652-PS. Moduli have been multiplied by 1, 10, 10^2, 10^3, and 10^4, respectively, for clarity of presentation.

These values are virtually identical to the values of the corresponding linear chains and consistent with the relevant literature values when compared to the same reference temperature.[21] The implication that linear and branched polymers exhibit the same WLF coefficients is rather important. However, a more detailed investigation is needed (including polymers with high degree of branching), before definite conclusions about similarities between linear and branched polymers are drawn.

III. Results and Data Analysis

In Figures 1 and 2 we present linear viscoelastic data for a series of linear comb homopolymer melts of two different chemistries (butadiene and styrene). As implied from Table 1, the number of entanglements varies from approximately 2 to 13 for the branches and 16 to 50 for the backbones, covering a very extensive range of molecular weights, whereas the number of branches ranges from 17 to 31. In the following, the data are often presented in the form of tangent of the phase angle ($\tan\delta = G''(\omega)/G'(\omega)$), which is more sensitive in distinguishing features of the relaxation processes. Figure 1 depicts the master curves for the PS c6-series combs of Table

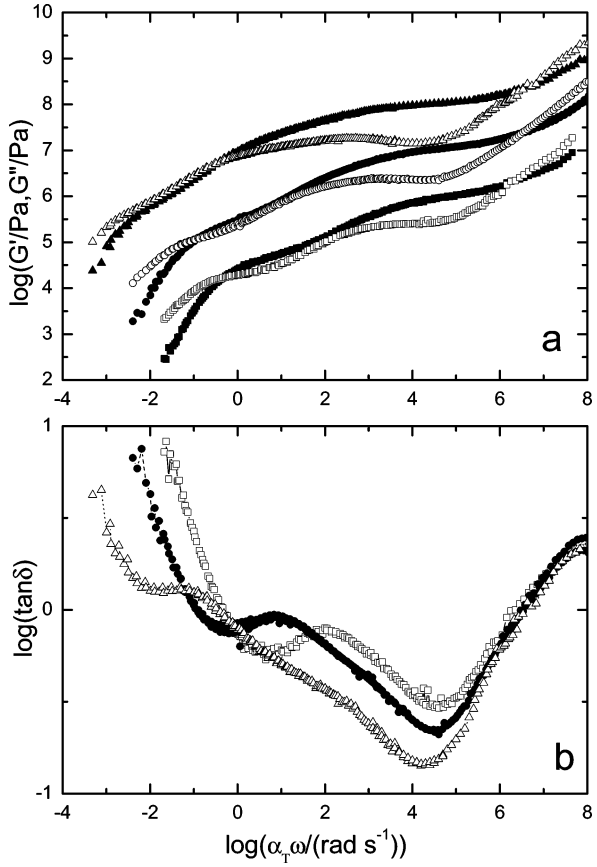

Figure 2. Linear rheology of PBd linear combs with equal backbone ($M_b = 50$ kg/mol) and increasing branch lengths. (a) The dynamic moduli and (b) the tangent of the phase angle: (■, □, and −□−) lc3-PBd, (●, ○, and −●−) lc1-PBd, (▲, △, and −△−) lc2-PBd. Moduli have been multiplied by 1, 10, and 10^2, respectively, for clarity of presentation.

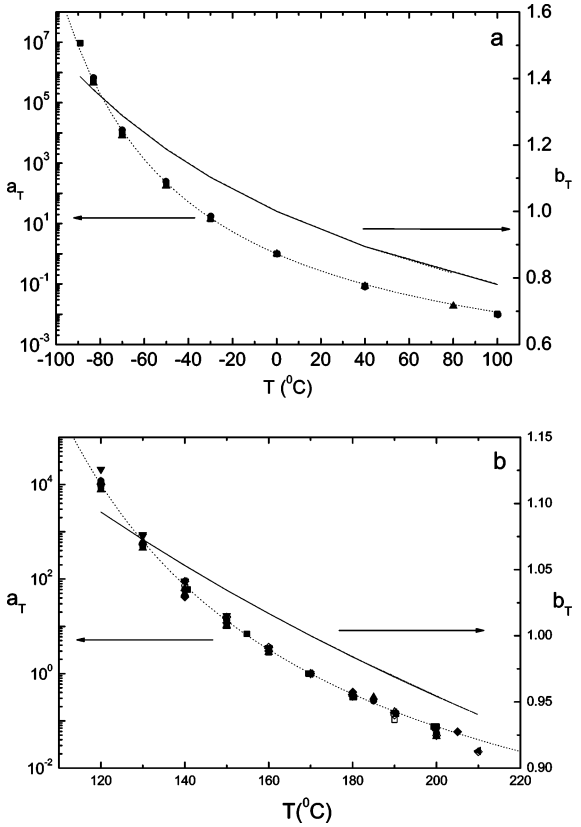

Figure 3. Horizontal (symbols) and vertical (lines) shift factors for (a) PBd and (b) PS linear combs. (a) (■) lc1-PBd; (●) lc2-PBd; (▲) lc3-PBd. (b) (○) c612-PS; (△) c622-PS; (▽) c632-PS; (◇) c642-PS; (tilted △) c642-PS; (■) c7bb; (●) c712-PS; (▲) c722-PS; (▼) c732-PS; (◆) c742-PS; (tilted ▲) c752-PS.

1, with virtually constant backbone and varying grafted branch molecular weight, as G', G'' vs ω (a) and tan δ vs ω (b). The respective data for the PBd combs are shown in Figure 2. From the inspection of the tan δ plots, it is evident that the high-frequency data collapse into one curve, as expected for local transitional Rouse-like and segmental motions, thus confirming the quality of data. At lower frequencies, in the plateau and terminal regions, each macromolecule with specific branch and backbone molecular weights has its own signature. Referring to Figure 1, samples c612-PS and c622-PS with unentangled branches, exhibit a single rubbery plateau (of the backbone), associated with the minimum in tan δ; this minimum marks the onset of backbone relaxation that proceeds to lower frequencies. As the branch degree of polymerization increases beyond the entanglement limit, we observe the onset of a relaxation at higher frequencies corresponding to the branches' disentanglements, in addition to the low-frequency terminal relaxation due to the backbone. Related to that, there are two rubbery plateaus, one relating to the branches just before they start relaxing and a second relating to the diluted (by the relaxed branches) backbone;[15] this is nicely identified in the tan δ plot as two minima. By comparing the frequency dependence of the moduli G', G'' and the phase angle tan(δ), it is evident that the latter is a very sensitive indicator of the appearance of the two relaxation processes (see Figures 1b and 2b). Further, from inspection of Figures 1 and 2 it can be observed that the terminal time and viscosity increase as a result of the increase of total weight of the polymer.

Returning to the lower frequency moduli attributed to the effective dilution of the backbone by the branches, for certain cases (combination of backbone molecular weight, grafted branch molecular weight, and number of grafted branches), the tan δ vs frequency curves exhibit a low-frequency plateau (c642-PS and c652-PS in Figure 1b; lc1-PBd and lc2-PBd in Figure 2b). This plateau reflects a power law behavior of the moduli, i.e., G', $G'' \propto \omega^n$ (Figures 1a and 2a), and for $n = 1/2$ it signifies an effective Rouse-like terminal relaxation of the backbone, as it is followed by the classical $G' \propto \omega^2$ and $G'' \propto \omega$.[4] Such a self-similar behavior with varying values of the exponent n, usually in the range $0 < n < 0.7$, has been associated with the behavior of critical gels,[23] and recently this kind of intermediate frequency response of branched polymers has been attributed to and correlated with critical gel behavior.[24,25] Despite this interesting correlation, we propose that this response can be rationalized in physically sound manner within the framework of the (full) dynamic dilution concept, as already discussed above; more specifically, as soon as the branches have retracted, they act as effective solvents and as a result the backbone tube swells, thus decreasing the effective number of its entanglements. Then, if the volume fraction of this effective solvent is large enough, the terminal motion may become that of a chain with few or virtually no entanglements, approaching the behavior of a Rouse chain. As an example, and in reference to Figures 1 and 2 for c642-PS and lc2-PBd, respectively, the diluted number of backbone

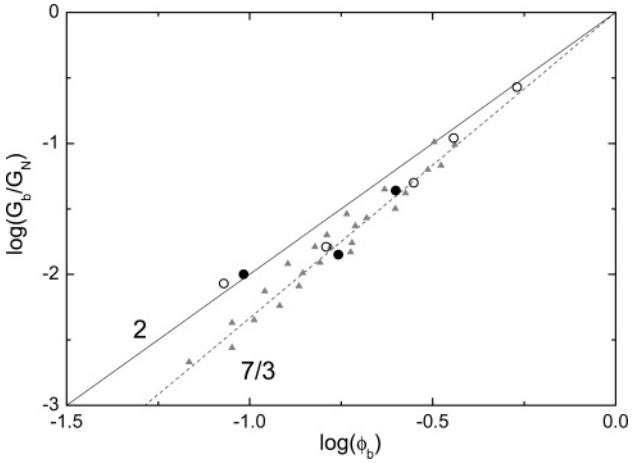

Figure 4. Ratio of the plateau moduli of the (diluted) backbone over the branches, G_b/G_N, against the volume fraction of the backbone in the entire comb molecule, ϕ_b. Ratios for both PBd (solid circles) and PS (open circles) are shown, obtained from Figures 1 and 2, respectively. The two theoretical slopes of 2 and $^7/_3$ are also indicated by the lines. Despite the use of $a = 1$, the model predictions (solid triangles) for monodisperse linear combs fall closer to the $^7/_3$ line.

entanglements is estimated to be 3 and 2.7 (for a dilution exponent $a = 1$; see also discussion below) or 1.6 and 1.4 (for a dilution exponent $a = {}^4/_3$).

A further manifestation of this dilution process is evidenced in Figure 4, which depicts the ratio of the two experimentally determined plateau moduli (diluted backbone, G_b, over branches, G_N) as a function of the backbone volume fraction in the entire comb molecule, ϕ_b (the theoretical predictions are discussed later). As the plateaus are not clearly observed in some cases, the G_b and G_N values reported are consistently determined from the G' corresponding to the minima of the tangent of loss angle. The universal behavior of both chemistries, PS and PBd comb polymers, is an important result. Moreover, it is clear that the ratio of the two moduli reflects the dilution effect of the first relaxed branches; this effect is enhanced as the volume fraction of the branches (i.e., their molecular weight and/or number) increases. However, despite the unambiguous qualitative signature of the effect, the present data are not sufficient to draw a definite quantitative conclusion with respect to the power law dependence of the G_b/G_N vs ϕ_b relationship, as they lie essentially between the two limiting predictions of 2 and $^7/_3$.[1,26–28]

IV. Complete Tube Model for Linear Comb Polymers

Within the framework of the tube model[1–4] and the hierarchical relaxation,[17] in a branched polymer the stress relaxation process starts from the free dangling ends and propagates toward the other parts of the chain. The relaxed parts do not contribute to the stress, and therefore they can be viewed as an effective solvent diluting the stress-carrying unrelaxed parts of the chain. This process is the so-called dynamic dilution, which changes with time (in contrast to the static, solvent-mediated dilution).[26] The plateau modulus can be written as $G_N(\phi) = G_N\phi^{\alpha+1}$ and the effective entanglement molecular weight $M_e(\phi) = M_e\phi^{-\alpha}$; the dilution exponent α assumes values 1 or $^4/_3$, depending on the approach.[27,28] Note that we use consistently the definition $M_e = (4/5)[\rho(T)RT/G_N(T)]$ throughout this work.

McLeish and co-workers have formulated a tube model with full dynamic dilution to describe the rheology of melts of H-polymers,[14] simple and asymmetric stars,[12,13,29] and linear combs.[15] Here we use the same concept and extend the model appropriately in order to test its success for a range of model combs as well as its possible limitations. In particular, the relaxation starts from the outer parts of the polymer, carrying dangling ends, i.e., the grafted branches and the ungrafted ends of the backbone; this is a starlike type of relaxation. During this time, the branch points are frozen in space, keeping the backbone frozen as well and partly stretched. The backbone is allowed to relax its stress only after the branches have fully relaxed. On the basis of this hierarchical scheme, the rheological response of the polymer can be split into different contributions, which are calculated independently. First is the high-frequency contribution, which is common for all segments and consists of two elements: the Rouse-like relaxation[4] and the longitudinal high-frequency motion, which reflects the initial segmental redistribution upon application of an instantaneous strain to the polymer.[8,30] Then, the branches relax first through end-point diffusion, and at later times the whole chain is involved in an activated retraction toward the branch point (typical star arm relaxation process).[12,13] Next, the branch points diffuse along the backbone, "exploring" their neighborhood, then retract toward the middle point ("two-arm star" behavior), and finally at long times they flow, here by reptating along the backbone tube. Therefore, the total relaxation modulus can be written as (the subscript "b" referring to the backbone contribution):

$$G^*_{\text{total}}(\omega) = G^*_{\text{high-freq}}(\omega) + G^*_{\text{branch}}(\omega) + G^*_{\text{b}}(\omega) \quad (1)$$

The above analysis is quite general and describes many branched systems, such as H-polymers,[14] combs,[15] and pom-pom molecules.[31] Depending on the actual architecture, the individual moduli expressions may differ of course. Below, we develop an expression for $G^*_{\text{total}}(\omega)$ of linear combs, using as starting point the earlier analysis of Daniels et al.[15] and introducing extensions or modifications where appropriate, in order to correct it, as discussed in the text.

IV.1. Relaxation of the Branches. As one may expect from the synthetic procedure,[18,19] branch points are randomly distributed along the backbone chain and not attached on its two ends. To date, this has been treated by uniformly distributing the branch points, essentially neglecting the part of the backbone near the tips (ends) and assuming that the effective part of the backbone that takes part into the motion is shorter than the actual.[15,19] In this work we treat that end part of the chain as an additional branch, not necessarily equal to the rest of the branches. All branches move simultaneously, but of course the shorter branches fully relax first before the longer ones. Frischknecht et al.[29] have partially addressed this problem. We compare the size of the crossbar (backbone) ends with that of the grafted branches and "label" the shorter ones as the "short" branches and the longer as the "long" branches. Accounting for both contributions yields the total branches modulus as the sum of the two terms:

$$G^*_{\text{branch}}(\omega) = G^*_{\text{long-branch}}(\omega) + G^*_{\text{short-branch}}(\omega) \quad (2)$$

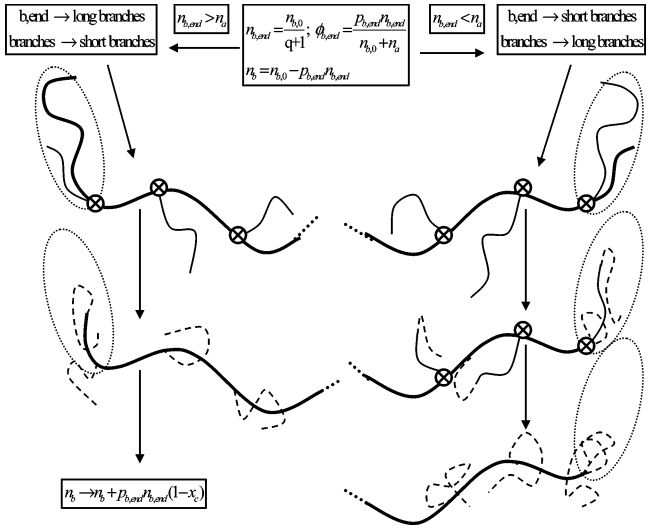

Figure 5. Schematic with the dangling branches relaxation depending on the relative sizes. b,end: backbone free ends; $p_{b,end}$: number of dangling ends per backbone (for linear combs $p_{b,end} = 2$).

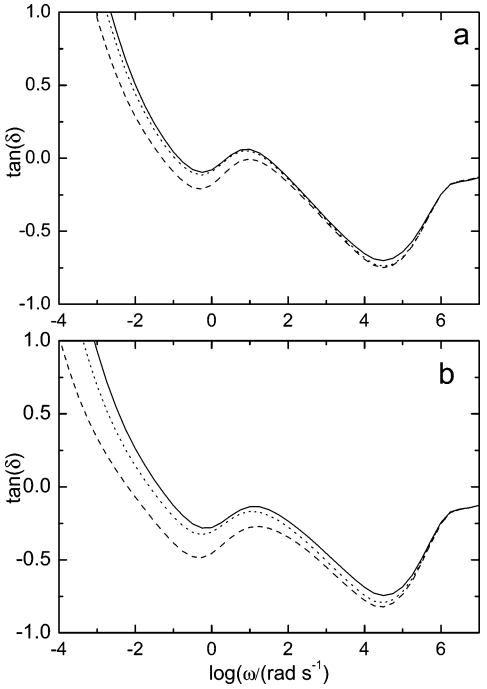

Figure 6. Theoretical predictions of the tan(δ) spectrum for linear combs with different treatment of the free side chains of the backbone: (−) as described in the text, referring to Figure 5; (− −) considering the whole, initial backbone length in the reptation process; (···) we ignore them completely and consider a smaller effective reptating backbone than the original. Figure parameters: (a) lc1-PBd parameters used; (b) lc1-PBd parameters, but with the number of branches halfed ($q = 9$).

The free (ungrafted) end of the backbone has an average molecular weight $M_{b,end} = M_{b,i}/(q + 1)$, where $M_{b,i}$ is the original (initial) backbone molecular weight (Table 1) and the "remaining" effective backbone molecular weight taking part in reptation is $M_{b,eff} = M_{b,i} - kM_{b,end}$, $k = 2$ for linear backbones. The characteristic crossover time τ_c, when all short branches have relaxed, is estimated by the condition $\tau_c = \tau_{long-branch}(x_c) = \tau_{short-branch}(1.0)$, where x_c is the crossover fractional distance along the long branch, equal to the short branch size; at the same time, since the short branches have relaxed, the respective value for them is 1. Before complete relaxation of the short branches, we have coexistence of both short and long branches. Beyond that point we have only one type of branches, the long ones.

The comparison between the grafted branches and the backbone ends is crucial and needs some further consideration. The cartoon of Figure 5 illustrates two possibilities: If the branches are longer than the backbone ends, then the branch points along the backbone (without its end parts) prevent it from moving, and thus the overall relaxation proceeds hierarchically (Figure 5, right; follow the motions within the dotted ellipses only). On the other hand, if the branches are shorter, they relax first and the remaining unrelaxed part of the backbone ends is added to the backbone that eventually reptates (Figure 5, left; again, follow the motions within the dotted ellipses only).

Details of the calculations of the times and moduli for the branch relaxation are provided in Appendix A. Figure 6 illustrates the results of a simple parametric study, which shows how the theoretical predictions change if the above effect of backbone ends is taken into account. The ends behave like branches, dynamically diluting the backbone, and thus make the relaxation faster. The effect becomes enhanced as the number of branches decreases, and thus the fraction of backbone distributed at the ends increases (Figure 6b).

IV.2. Backbone Relaxation. In the full dilation picture adopted here, the branch relaxation yields an effective (dilated) backbone tube diameter $a_{b,eff} = a_b\phi^{-\alpha/2}$. Since the ends are free to move, the linear backbone relaxes as an effective two-arm star (we take the values of the degree of polymerization and number of branches per "arm" as $N_b = N_{b,eff}/2$ and $q = q_i/2$, where the subscript "i" refers to the initial values of the original backbone, based on Table 1) inside the dilated tube. The related early time calculation is described in Appendix B. For the activated process we follow the procedure used in the analysis of the stars:[12,13]

$$\tau_{late}(x_b) = \frac{L^2}{D_{eff}}\int_0^{x_b} ds\, e^{U_b(s)} \int_{-\infty}^{s} dt\, e^{-U_b(t)},$$

$$\text{with } \frac{L^2}{D_{eff}} = \frac{(n_b a_{b,eff,b} \phi_b{}^{\alpha})^2}{\frac{p^2 a_{eff,b}{}^2}{2\tau_a(1)}} = \frac{2}{p^2} n_b{}^2\, \phi_b{}^{2\alpha} \tau_a(1) \quad (3)$$

$$U(x_b) = 3\left(\frac{N_b}{N_e \phi_b{}^{-\alpha}}\right) \frac{1 - (1 - x_b)^{\alpha+1}[1 + (1 + \alpha)x_b]}{(1 + \alpha)(2 + \alpha)} \quad (4)$$

The double integral is calculated numerically if $n_b = M_b/M_e \leq 5$; this allows relaxing the constraint of the model that all chains need to be well entangled.

Reptation enters into the picture last. It is the mechanism for relaxing the remaining stress of the backbone. It takes over as soon as $\tau_b(x_b)$ becomes larger (slower) than τ_d. The equation for the determination of the critical size x_d is

$$\tau_b(x_d) = \tau_d = \frac{2q}{\pi^2 p^2}\, \tau_a(1)(n_b \phi_b{}^{\alpha})^2 (1 - x_d)^2 \quad (5)$$

where the (unknown) adjustable parameter p^2 describes the extend of diffusion of the branch point, in terms of fraction of the effective tube diameter, a_{eff}; the diffusion

coefficient is given by $D_{\text{eff}} = (pa_{\text{b,eff}})^2/2\tau$, where τ is the branch (arm) retraction time.[1,15,32] From the early and activated times the overall relaxation time of the backbone is obtained:

$$\tau_{\text{b}}(x_{\text{b}}) = \frac{\tau_{\text{early}}(x_{\text{b}})\tau_{\text{late}}(x_{\text{b}})\text{e}^{U(x_{\text{b}})}}{\tau_{\text{early}}(x_{\text{b}})\text{e}^{U(x_{\text{b}})} + \tau_{\text{late}}(x_{\text{b}})} \tag{6}$$

The corresponding backbone contribution to stress is then

$$G^*_{\text{b}}(\omega) = (a+1)G_N\phi_{\text{b}}^{a+1}\left[\int_0^{x_{\text{d}}}\text{d}s\,(1-s)^a\frac{i\omega\tau_{\text{b}}(s)}{1+i\omega\tau_{\text{b}}(s)} + \frac{(1-x_{\text{d}})^{a+1}}{a+1}\sum_{n,\text{odd}}\frac{8}{\pi^2n^2}\frac{i\omega\tau_{\text{d}}/n^2}{1+i\omega\tau_{\text{d}}/n^2}\right] \tag{7}$$

IV.3. High-Frequency Modes. The high-frequency motions ($\omega \geq 1/\tau_{\text{e}}$) that follow Rouse dynamics are given by

$$G_{\text{R}}(t) = \frac{G_N}{n - nM_0/M_{\text{e}}}\sum_{n=M/M_{\text{e}}}^{M/M_0}\exp\left[-2n^2\frac{t}{\tau_{\text{R}}}\right] = \frac{G_N}{1-M_0/M_{\text{e}}}\sum_{m=1}^{M_{\text{e}}/M_0}\exp\left[-2m^2\frac{t}{\tau_{\text{e}}}\right]$$

Thus, the respective Fourier transform becomes

$$G^*_{\text{R}}(\omega) = \frac{G_N}{1-M_0/M_{\text{e}}}\sum_{m=1}^{M_{\text{e}}/M_0}\frac{i\omega\tau_{\text{e}}}{2m^2+i\omega\tau_{\text{e}}} \tag{8}$$

In this time range the segments do not feel the tube yet, and the result does not depend on the chain length.

Additionally, we include the longitudinal modes[8,30] for the dangling branches, which correspond to the reorientation of the segments due to the applied strain. As the branch points keep the backbone essentially frozen, we assume that only the branches and the backbone ends, i.e., long and short branches of section IV.1, possessing free dangling ends, contribute to this mode of stress relaxation. The resulting modulus is given by

$$G^*_{\text{longutudinal}}(\omega) = \frac{G_N}{4}\left[\frac{\phi_{\text{s}}}{n_{\text{s}}}\sum_{p=0}^{n_i-1}\frac{in_{\text{s}}{}^2\omega\tau_{\text{e}}}{(p+{}^1\!/_2)^2+in_{\text{s}}{}^2\omega\tau_{\text{e}}} + \frac{\phi_l}{n_l}\sum_{p=0}^{n_i-1}\frac{in_l{}^2\omega\tau_{\text{e}}}{(p+{}^1\!/_2)^2+in_l{}^2\omega\tau_{\text{e}}}\right] \tag{9}$$

IV.4. Polydispersity. There are three different kinds of polydispersity that enter into the problem of comb relaxation and need consideration, namely the size variance of the grafted branches, that of the backbones, and the ambiguity in the number as well as the position of branches; all uncertainties generate polydispersity in the total molecular weight of the comb polymer. According to synthesis procedure,[18,19] the size polydispersity ($M_{\text{w}}/M_{\text{n}}$) of the individual chains is not more than 1.07. By assuming that the branches are equidistant on the backbone (which is reasonable on the average and accounts for the position distribution of the branches), problems may arise from the distribution in the chain sizes and the number of branches.

Polydispersity in size affects the relaxation time so it can be estimated indirectly as done by Frischknecht et al.[29] To a first approximation, this results in increasing by a small fraction the corresponding chain size. However, this is rather crude analysis which has only limited use. We are following a more direct procedure, which is computationally intensive, but more general and accurate. We assume a Schulz−Zimm distribution function that describes the polydispersity $w(N)$ for a quantity, N:

$$w(N) = \frac{1/N}{\Gamma(\beta)}\left(\frac{\beta N}{\langle N\rangle}\right)^{\beta}\exp\left[-\frac{\beta N}{\langle N\rangle}\right]$$

with

$$\int \text{d}N\,w(N) = 1 \quad \text{and} \quad \frac{N_{\text{w}}}{N_{\text{n}}} = \epsilon_N = 1 + \frac{1}{\beta}$$

Thus, by tuning the parameter β, one can control the polydispersity index. We "construct" polymers by independently varying the branch and backbone size (M_{a} and M_{b}, respectively) and the number of branches (q), and then the final result is the average of all possible conformations weighted according to the distributions.

The total modulus is calculated as

$$G^*(\omega) = \sum_{M_{\text{b}}}\sum_{M_a}\sum_{q} w(M_{\text{a}})\,w(M_{\text{b}})\,w(q)\,G^*(M_{\text{b}},M_{\text{a}},q;\omega) \tag{10}$$

Note that the number of branch points, q, needs to be an integer number, and this produces some technical difficulties in the discretization process, in the sense that we ensure a bell-like shape distribution with $\langle q\rangle = q$ but not precisely of Schulz−Zimm type (rather, a wider bell-shape discrete distribution). However, this does not affect the outcome as long as its values are not close to unity ($q > 4$).

Figure 7 illustrates the prediction of the model concerning the effects of polydispersity on the comb relaxation. As expected, the high-frequency branch of the relaxation spectrum is unaffected by the variation in M_{a}, M_{b}, or q. On the other hand, it is evident that even a small degree of polydipsersity can have a significant impact on the linear viscoelastic spectrum, in the intermediate and especially the lower frequencies, and thus it should be accounted for. Larger polydispersity (dotted lines in Figure 7) smoothens and disperses the single mode transitions (expressed by the sharp extrema of the loss angle tangent). This is a qualitative difference from the approach proposed by Frischknecht et al.,[29] which effectively increases the chain size in order to reach a longer relaxation time.

V. Comparison of Data with Theoretical Model

As explained in section IV, the original model of Daniels et al.[15] has been modified in order to account for a variety of situations and effects of the synthetic procedure, such as smaller number of entanglements and branches per chain, dangling ends of backbone, and high-frequency contributions. To compare the experimental data with the model, we need a number of parameters; besides the a and p^2 which are discussed

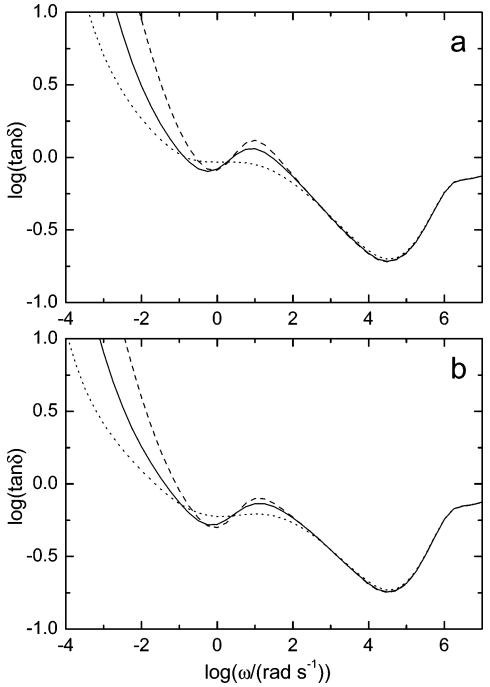

Figure 7. Theoretical predictions of the polydispersity effect: Parameters used are those of (a) lc1-PBd and (b) lc1-PBd parameters, but with the number of branches halfed ($q = 9$). Lines: (– –) ($\epsilon_a = 1.01$, $\epsilon_b = 1.01$, $\epsilon_q = 1.01$); (—) ($\epsilon_a = 1.03$, $\epsilon_b = 1.06$, $\epsilon_q = 1.01$); (···) ($\epsilon_a = 1.10$, $\epsilon_b = 1.10$, $\epsilon_q = 1.01$).

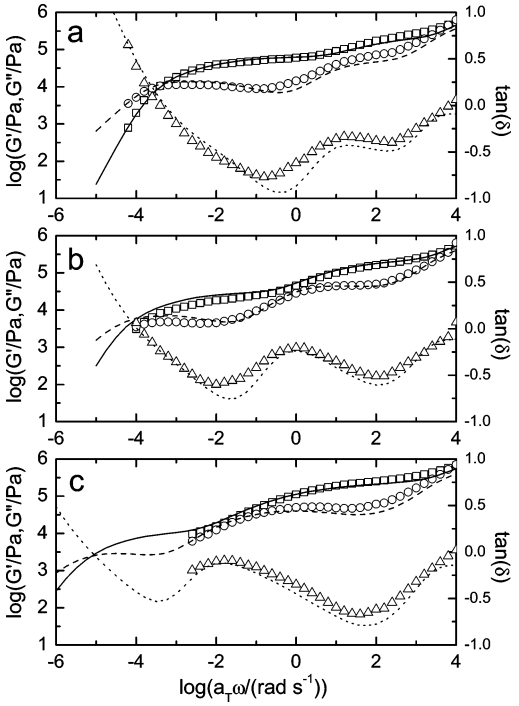

Figure 8. Dynamic moduli (G′ □, G″ ○) and tangent of phase lag (△) fitted (lines) for (a) c732-PS ($\epsilon_a = 1.04$, $\epsilon_b = 1.01$, $\epsilon_q = 1.01$), (b) c742-PS ($\epsilon_a = 1.03$, $\epsilon_b = 1.01$, $\epsilon_q = 1.01$), and (c) c752-PS ($\epsilon_a = 1.02$, $\epsilon_b = 1.01$, $\epsilon_q = 1.01$).

below, the other parameters are obtained directly from the chemical characterization and rheological data (see Table 2).

From the synthesis, the molecular characteristics (branch and backbone sizes, degree of branching) are given (Table 1). On the basis of the experimental frequency spectrum, we obtain the values of the characteristic Rouse time of an entanglement, τ_e (the time where the G' Rouse line with slope $^1/_2$ that fits high-frequency data intersects the plateau modulus[33]), the plateau modulus, and the entanglement molecular weight that are listed in Table 2 and give very good and consistent fits (discussed below). We note that the latter values, M_e and G_N, obey the expression $M_e = (4/5)[\rho(T)RT/G_N(T)]$ and are very close to the literature values (within 25% or better).[21,34]

We have chosen a dilution exponent of $\alpha = 1$ as fits using this value produce consistently more reasonable results. In fact, this can be also confirmed by inspection of Figure 4. In this figure we have calculated the dependence of the ratio G_b/G_N (from the tan δ minimum, in harmony with the data analysis) on the backbone volume fraction, ϕ_b. It is interesting that with $a = 1$ in all cases the model predictions are closer to the $^7/_3$ slope. This apparent inconsistency is due to the level of sophistication of the model, but the key message is the model's ability to predict the experimental observations.

The only remaining parameter is p^2, an adjustable one. In this work, it takes a fixed value of 1/12, which is similar to values reported in previous works;[14,15,29,35] however, we are still missing a thorough account of its physical significance.

New elements in this work include the two separate chemistries: the wide variation in the number of entanglements (reaching much lower values compared to other works) and the model modifications/extensions. Furthermore, the number of branch points is quite large in all cases considered here, and the calculation of the backbone early times is discussed accordingly in Appendix B and ref 15. Of course, the model does not apply to samples with unentangled grafted branches.

Figure 8 shows the theoretical fits to the experimental data of the PS combs with the higher molecular weight per backbone (c7 series). The fits are good, even for branches with few entanglements, suggesting that the modified model is quite successful. A more interesting result is presented in Figure 9, where for a different chemistry (PBd) satisfactory fits are obtained as well. We note in particular that, by observing the more sensitive tan(δ) spectrum, one can conclude that the model is very successful in qualitatively capturing the two mechanisms of relaxation (branches and backbones, reflected as the two local minima in the plots), confirming the validity of the concept of hierarchical motions in this type of architecturally complex macromolecules. On the other hand, the quantitative comparison is not perfect.[36] One should also bear in mind that, with the exception of a and p^2, all molecular parameters are directly obtained from the rheological experiments or

Table 2. Molecular Features and Parameters Used in the Fitting Procedure

polymer	$\rho(T_{ref})$ (kg/m^3)	log(G_N/Pa)[a]	M_e (kg/mol)	M_e^{*b} (kg/mol)	log(τ_e/s)	α	p^2
PBd	902	6.05	1.46	1.825	−6.25 to −6	1	1/12
PS	982	5.40	11.50	14.38	−3.5 to −3.3	1	1/12

[a] Literature G_N plateau values for PS and PBd are $10^{5.3}$ and $10^{6.05}$ Pa, respectively (from refs 18 and 19, where G_N was determined from the integration of G''). [b] The M_e^* values are obtained from the experimental M_e using the definition in Ferry's textbook,[21] i.e., without the 4/5 prefactor.

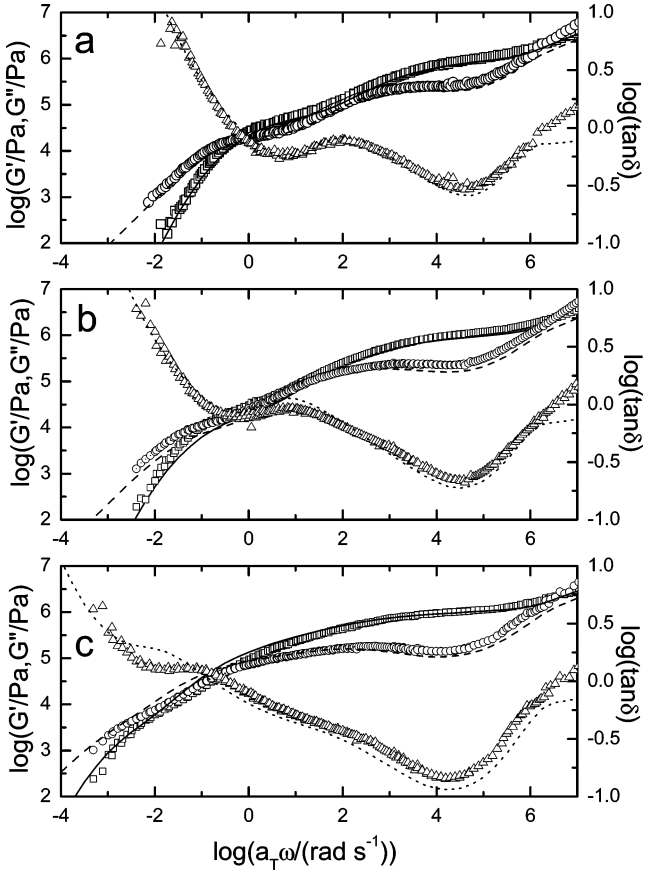

Figure 9. Dynamic moduli (G′ □, G″ ○) and tangent of phase lag (△) fitted (lines) for (a) lc3-PBd ($\epsilon_a = 1.05$, $\epsilon_b = 1.03$, $\epsilon_q = 1.01$), (b) lc1-PBd ($\epsilon_a = 1.01$, $\epsilon_b = 1.01$, $\epsilon_q = 1.01$), and (c) lc2-PBd ($\epsilon_a = 1.01$, $\epsilon_b = 1.01$, $\epsilon_q = 1.01$).

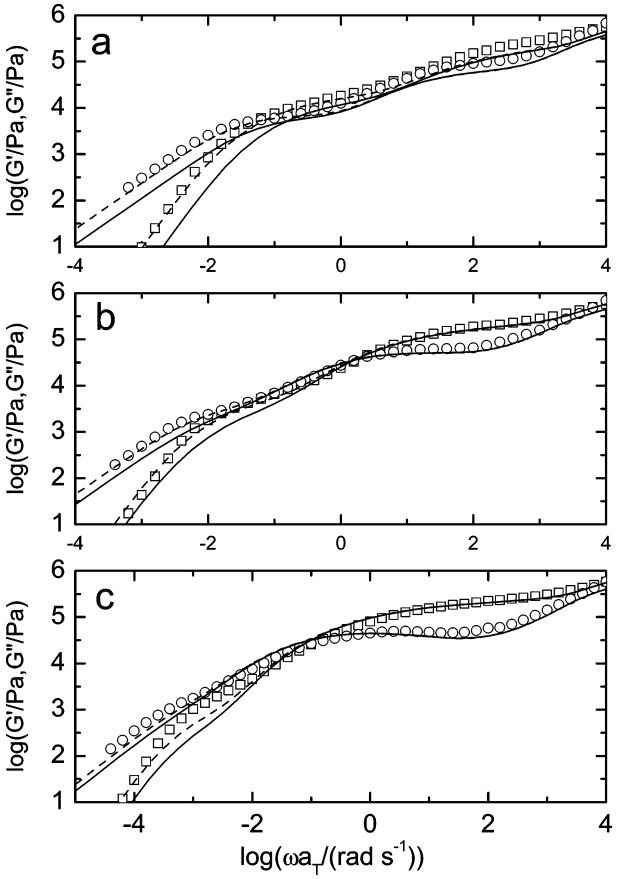

Figure 10. Dynamic moduli (G′ □, G″ ○) for c6-PS series with stretched backbone due to large number of branches ($N_b/(q + 1) \approx 0.68$). Solid lines are fits with the nominal values of the parameter, while dashed lines are fits after increasing the backbone length by 16%. (a) c632-PS ($\epsilon_a = 1.06$, $\epsilon_b = 1.02$, $\epsilon_q = 1.01$), (b) c642-PS ($\epsilon_a = 1.06$, $\epsilon_b = 1.03$, $\epsilon_q = 1.01$), and (c) c652-PS ($\epsilon_a = 1.01$, $\epsilon_b = 1.05$, $\epsilon_q = 1.01$).

the chemical characterization. Therefore, attention shifts to these two more ambiguous ones. Concerning the scaling exponent a, in fact the dilution is not a fully resolved issue. Recent studies suggest contradicting results,[27,28,30,37,38] and here we use a fixed value $a = 1$ that provides consistently a very reasonable overall description of the experimental data. The parameter p^2, which is related to the branch point friction, is a more difficult issue. The fact that the presented fits were obtained with a constant value of p^2 for both chemistries and similar to some earlier works, as already mentioned,[14,15,29,35] but not all,[29,35,39] is interesting but not much encouraging with respect to a further elaboration of this issue. At this point, it should be noted, however, that the full tube dilation framework, on which this analysis is based, may not be completely valid. It is known that dynamic dilution is not the only approach to describe the constraint release process.[8,26,40−43] There is already clear evidence in the literature that the dynamic dilution breaks down for in entangled linear blends and star chains,[44,45] and so it is expected that it may break down for more complicated architectures as well; what is not known is at which point it will break down.[46] All in all, the combination of the dynamic dilution with the chosen values of the parameters and p^2 results in the good results of this work. However, we propose that further elaboration of this problem requires a combined investigation of these two factors (friction parameter and dilution exponent) in conjunction with the tube dilation issue to obtain an improved picture. At this stage we speculate that they "absorb" some of the dilution effect.

A final remark is in order, concerning the case of smaller backbone molecular weight and the same number of branches (c6-PS series); in this case, the average number of entanglements between two branches is defined as $\bar{n} = n_b/(q + 1)$. For these polymers, the calculated $\bar{n}$ is actually below unity, suggesting a type of polymacromonomeric structure.[47] Under these stereochemical conditions, the backbone may not retain its equilibrium Gaussian conformation, but it may be slightly elongated instead, and this may be the reason for the poor agreement of the model with the data (see Figure 10). The implication is that the effective backbone length may be enlarged, but on the other hand, since for situations involving non-Gaussian chains, the model should be revised in several aspects.[48] Here, we only show with a simplistic back-of-the-envelope calculation that this possibility of a partial backbone chain extension seems to work. In particular, if we forget for the moment the possible non-Gaussian behavior, and consider only the enlargement (which in a very rough way relates to an effective increase of the molecular weight), we can calculate the resulting moduli; we show in Figure 10 that a 16% increase of the backbone length is sufficient to consistently improve all fits to an almost perfect agreement with experiments. Of course, this issue requires further elaboration that is beyond the scope of the present contribution, but at this stage we believe that this empirical observation is interesting.

VI. Conclusions

We have measured the linear rheology of model PBd and PS comb homopolymer melts. We have appropriately modified and extended the tube theory of Daniels et al.[15] within the full dynamic dilution framework to account for several aspects of the synthetic procedure (dangling backbone ends, polydispersity) as well as the low number of entanglements and have also included the high-frequency modes. Our results from the comparison of data and the complete model confirm the validity of the hierarchical scheme of relaxation in such architecturally complex macromolecules. To accomplish this, all molecular parameters were determined self-consistently from the present rheological data or the chemical characterization of the model polymers.[18,19] The only two exceptions is the dilution exponent a and the friction parameter p^2, which assumed fixed values of 1 and 1/12, respectively. On the basis of the ability of the model to capture the data (with very good quantitative agreement in most cases, for both chemistries), the chosen values of a and p^2 are considered reasonable and the model successful. However, we propose as a further step that the physical significance of the range of dynamic dilution should be considered in conjunction with these two parameters. Nevertheless, we believe that in its present form the analysis presented here with its shortcomings (because of the slight ambiguity with a and p^2) signifies progress in the understanding of the rheology of linear comb polymers.

Acknowledgment. We thank Alexei Likhtman and Tom McLeish for many valuable discussions, Ralph Colby for insightful comments and suggestions, and Irene Chira for technical assistance. This work was partially supported by the E.U (NMP3-CT-2004-502235).

Appendix A. Calculation of the Branches Relaxation

The total time entering the integrations follows the usual blending rule seen in all papers describing this model:

$$\frac{1}{\tau_i(x)} = \frac{1}{\tau_{\text{early},i}(x)\mathrm{e}^{U_i(x)}} + \frac{1}{\tau_{\text{late},i}(x)} \Rightarrow \tau_i(x) = \frac{\tau_{\text{early},i}(x)\tau_{\text{late},i}(x)\mathrm{e}^{U_i(x)}}{\tau_{\text{early},i}(x)\mathrm{e}^{U_i(x)} + \tau_{\text{late},i}(x)} \quad \text{(A.1)}$$

This mixing ensures that the chain will always prefer relaxing through the fastest process.

The volume fraction of unrelaxed chains at time $\tau_i(x_i)$ is

$$\Phi = \begin{cases} \phi_b + \phi_s(1-x_s) + \phi_l(1-x_l) & x_s < 1,\ \tau_i(x_i) < \tau_c \\ \phi_b + \phi_l(1-x_l) & \tau_i(x_i) > \tau_c \end{cases} \quad \text{(A.2)}$$

with $\phi_b + \phi_s + \phi_l = 1$. Assuming random walk (Gaussian chain), we are making a convenient change of variables: $y = n_l x_l^2 = k^2 n_s x_s^2$. The nonphysical constant k serves for the change of variables and will be determined later. Then

$$\frac{\mathrm{d}}{\mathrm{d}x_i}\ln\tau_i(x_i) = 3n_i x_i \Phi^{\alpha} = \frac{\mathrm{d}U_{\text{eff},i}(x_i)}{\mathrm{d}x_i}$$

(where $i = s, l$), with a change of variables can be written

$$\frac{\mathrm{d}}{\mathrm{d}y}\ln\tau_l(y) = \frac{3}{2}\Phi(y)^{\alpha} = \frac{\mathrm{d}U_{\text{eff},l}(y)}{\mathrm{d}y}$$

and

$$\frac{\mathrm{d}}{\mathrm{d}y}\ln\tau_s(y) = \frac{3}{2}\frac{\Phi(y)^{\alpha}}{k} = \frac{\mathrm{d}U_{\text{eff},s}(y)}{\mathrm{d}y}$$

Solution of the equation for long branches gives

$$U_{\text{eff},l}(x_l) = \begin{cases} 3n_l \dfrac{1-(1-g_l x_l)^{a+1}[1+(1+a)g_l x_l]}{g_l^2(1+a)(2+a)}, \\ \qquad g_l = \phi_l + \dfrac{\phi_s}{k}\sqrt{\dfrac{n_l}{n_s}} & x_l \le x_c \\ \left(1+\dfrac{\phi_b}{\phi_l}\right)^{a+2} - \\ 3n_l\phi_l^a \dfrac{\left(1+\dfrac{\phi_b}{\phi_l}-x_l\right)^{a+1}\left[1+\dfrac{\phi_b}{\phi_l}+(1+a)x_l\right]}{(1+a)(2+a)} + c & x_l > x_c \end{cases} \quad \text{(A.3)}$$

And for short branches

$$U_{\text{eff},s}(x_s) = 3n_s \frac{1-[1-g_s x_s]^{a+1}[1+(1+a)g_s x_s]}{g_s^2(a+1)(a+2)}$$

with

$$g_s = \phi_s + k\phi_l\sqrt{\frac{n_s}{n_l}} \quad \text{(A.4)}$$

The constant k is determined from the need that $U_{\text{eff},s}(1) = U_{\text{eff},l}(x_c) \Rightarrow k = x_c\sqrt{n_l/n_s} \Rightarrow g_s = \phi_s + x_c\phi_l$ and $g_l = \phi_l + \phi_s/x_c$. The constant c is determined from continuity condition of the potential. The characteristic time τ_c is calculated from $\tau_c = \tau_{\text{long-arms}}(x_c) = \tau_{\text{short-arms}}(1.0)$.

The early time is

$$\tau_{\text{early},i}(x) = \frac{9}{16}\pi^3 n_i^4 \tau_e x^4 \quad \text{(A.5)}$$

where $n_i = M_i/M_e$, i = short branches or long branches.

The late time is calculated by

$$\tau_{\text{late},i}(x_i) = \frac{L_i^2}{D_{i,\text{eff}}}\int_0^{x_i}\mathrm{d}q_1\,\mathrm{e}^{U_i(q_1)}\int_{-\infty}^{q_1}\mathrm{d}q_2\,\mathrm{e}^{-U_i(q_2)} \quad \text{(A.6)}$$

with $L_i^2/D_{i,\text{eff}} = (3\pi^2/2)n_i^3\tau_e$. $D_{\text{eff},i}$ is the effective curvilinear diffusion constant of the retracting branch in its tube. Most authors use an approximation for the double integral assuming that s_i is very high.[12,28] However, if this assumption does not hold, the result is not accurate. In this work, the term $\tau_{\text{late},i}(x_i)$ in eq A.6 is calculated numerically. Moreover, we note that in the work of Frischknecht et al.[28] because of this approximation $\tau_l(x)$ is discontinuous function (the two branches are unequal at $x_l = x_c$). This unphysical effect is cured when the double integral is calculated numerically.

The characteristic time when all short chains have fully relaxed is determined from $\tau_c = \tau_l(x_c) = \tau_s(1.0)$. Finally, the moduli are written

$$G^*_{\text{short-branch}}(\omega) = (a+1)G_N\phi_s\int_0^1 \mathrm{d}s\,(1-g_s s)^a \frac{i\omega\tau_s(s)}{1+i\omega\tau_s(s)} \quad \text{(A.7)}$$

$$G^*_{\text{longbranch}}(\omega) = (a+1)G_N\left[\phi_l\int_0^{x_c}\mathrm{d}s\,(1-g_l s)^a\frac{i\omega\tau_l(s)}{1+i\omega\tau_l(s)} + \phi_l^{\,a+1}\int_{x_c}^1\mathrm{d}s\left(1+\frac{\phi_b}{\phi_l}-s\right)^a\frac{i\omega\tau_l(s)}{1+i\omega\tau_l(s)}\right] \quad \text{(A.8)}$$

Appendix B. Backbone Early Time Calculation

As already mentioned in ref 15, we need to differentiate between taking small and large number of branches. After the branch relaxation and for high to moderate number of branches along the backbone, we assume that we have an array of effective blobs connected with springs. The blobs correspond to the relaxed branches.

The effective tube diameter is formed from other backbones with relaxed branches and due to geometrical reasons now scales as $a_{b,\text{eff}} = b\sqrt{N_{e,\text{eff}}} = b\sqrt{N_e/\phi^a} = a_b\phi^{-a/2}$.

From 1-d random walk we get $\langle s^2(t)\rangle = 2Dt \Rightarrow \Delta t = a^2/2D$. The friction comes from the blobs. In our model this gives $D_b = k_BT/\zeta = p^2[a_{b,\text{eff}}{}^2/(2\tau_{\text{branch}}(x_a=1)]$, where p^2 is a constant of order unity to compensate for the approximations in the formula. Then, the new Kuhn segment is $b_{\text{new}}{}^2 = (N_b/q)b^2$, and thus the new Rouse time is $\tau_R = (\zeta/3\pi^2k_BT)[(N_b/q)b^2]q^2$, where q is the number of blobs. (Note that for the linear backbone we have $N_b = N_{b,i}/2$ and $q = q_i/2$, where the subscript "i" refers to the initial values, Table 1).

Again we use the same early time equation $\tau_{\text{early}}(x_b) = (9/16)\pi^3(N_b/N_e\phi^{-a})^2\tau_R x_b{}^4$, and substituting we obtain

$$\tau_{\text{early}}(x_b) = \frac{3\pi}{8p^2}q(n_b\phi_b{}^a)^3\tau_a(1)x_b{}^4 \quad \text{(B.1)}$$

On the other hand, if the number of branches per backbone is very small (a situation not addressed experimentally here), then all friction mass is concentrated in blobs that can be considered independent. For an isolated particle we have

$$\langle\Delta R^2\rangle = 2D_R\tau_R(1-\mathrm{e}^{-t_{be}/\tau_R}) \sim 2D_R t_{be}$$

$$D_R = \frac{D_{b,\text{eff}}}{q} = p^2\frac{a_{b,\text{eff}}{}^2}{2q\tau_{\text{branch}}(x_a=1)}$$

and

$$\langle\Delta R^2\rangle = x_b{}^2\frac{L_{b,\text{eff}}{}^2}{4} = \frac{x_b{}^2}{4}\left(\frac{N_b a\phi^{-a/2}}{N_e\phi^{-a}}\right)^2 = \frac{x_b{}^2}{4}n_b{}^2a^2\phi^a$$

Substitution gives[49]

$$\tau_{\text{early}}(x_b) = \frac{1}{4p^2}q(n_b\phi_b^a)^2\tau_a(1)x_b{}^2 \quad \text{(B.2)}$$

References and Notes

(1) McLeish, T. C. B. *Adv. Phys.* **2002**, *51*, 1379.
(2) Watanabe, H. *Prog. Polym. Sci.* **1999**, *24*, 1253.
(3) Marrucci, G.; Greco, F.; Ianniruberto, G. *Curr. Opin. Colloid Interface Sci.* **1999**, *4*, 283. vanRuymbeke, E.; Keunings, R.; Stephenne, V.; Hagenaars, A.; Bailly, C. *Macromolecules* **2002**, *35*, 2689. Evaraers, R.; Sukumaran, S. K.; Grest, G. S.; Svaneborg, C.; Sivasubramanian, A.; Kremer, K. *Science* **2004**, *303*, 823.
(4) Doi, M.; Edwards, S. F. *The Theory of Polymer Dynamics*; Oxford University Press: New York, 1986.
(5) Hsieh, H. L.; Quirk, R. P. *Anionic Polymerization: Principles and Practical Applications*; Marcel Dekker: New York, 1996.
(6) Pitsikalis, M.; Pispas, S.; Mays, J. W.; Hadjichristidis, N. *Adv. Polym. Sci.* **1998**, *135*, 1.
(7) Hadjichristidis, N.; Pitsikalis, M.; Pispas, S.; Iatrou, H.; Vlahos, C. *Adv. Polym. Sci.* **1999**, *142*, 71.
(8) Likhtman, A. E.; McLeish, T. *Macromolecules* **2002**, *35*, 6332.
(9) Hatzikiriakos, S. G. *Polym. Eng. Sci.* **2000**, *40*, 2279. Janzen, J.; Colby, R. H. *J. Mol. Struct.* **1999**, *485*, 569. Larson, R. G. *Macromolecules* **2001**, *34*, 4556.
(10) Aggeli, A.; Bell, M.; Boden, N.; Keen, J. N.; McLeish, T. C. B.; Nyrkova, I.; Radford, S. E.; Semenov, A. *J. Mater. Chem.* **1997**, *7*, 1135. Kaes, J.; Strey, H.; Sackmann, E. *Nature (London)* **1994**, *368*, 226. Hinner, B.; Tempel, M.; Sackmann, E.; Kroy, K.; Frey, E. *Phys. Rev. Lett.* **1998**, *81*, 2614. MacKintosh, F. C.; Kaes, J.; Janmey, P. A. *Phys. Rev. Lett.* **1995**, *75*, 4425.
(11) Fetters, L. J.; Kiss, A. D.; Pearson, D. S.; Quack, G. F.; Vitus, F. J. *Macromolecules* **1993**, *26*, 647.
(12) Milner, S. T.; McLeish, T. C. B. *Macromolecules* **1997**, *30*, 2159.
(13) Milner, S. T.; McLeish, T. C. B. *Macromolecules* **1998**, *31*, 7479.
(14) McLeish, T. C. B.; Allgaier, J.; Bick, D. K.; Bishko, G.; Biswas, P.; Blackwell, R.; Blottiere, B.; Clarke, N.; Gibbs, B.; Groves, D. J.; Hakiki, A.; Heenan, R. K.; Johnson, J. M.; Kant, R.; Read, D. J.; Young, R. N. *Macromolecules* **1999**, *32*, 6734.
(15) Daniels, D. R.; McLeish, T. C. B.; Crosby, B. J.; Young, R. N.; Fernyhough, C. M. *Macromolecules* **2001**, *34*, 7025.
(16) Blackwell, R. J.; Harlen, O. G.; McLeish, T. C. B. *Macromolecules* **2001**, *34*, 2579.
(17) McLeish, T. C. B. *Europhys. Lett.* **1988**, *6*, 511.
(18) Roovers, J.; Graessley, W. W. *Macromolecules* **1981**, *14*, 766. Roovers, J. *Polymer* **1979**, *20*, 843.
(19) Roovers, J.; Toporowski, P. *Macromolecules* **1987**, *20*, 2300.
(20) Fetters, L. J.; Lohse, D. J.; Richter, D.; Witten, T. A.; Zirkel, A. *Macromolecules* **1994**, *27*, 4639.
(21) Ferry, J. D. *Viscoelastic Properties of Polymers*, 3rd ed.; Wiley: New York, 1980.
(22) Zoller, P., Walsh, D., Eds.; *Standard Pressure−Volume−Temperature Data for Polymers*; Technomic Publishing Co.: New York, 1995.
(23) Winter, H. H.; Mours, M. *Adv. Polym. Sci.* **1997**, *137*, 165.
(24) Garcia-Franco, C. A.; Srinivas, S.; Lohse, D. J.; Brant, P. *Macromolecules* **2001**, *34*, 3115.
(25) Robertson, C. G.; Garcia-Franco, C. A.; Srinivas, S. *J. Polym. Sci., Part B: Polym. Phys.* **2004**, *42*, 1671.
(26) Ball, R. C.; McLeish, T. C. B. *Macromolecules* **1989**, *22*, 1911. Marrucci, G. *J. Polym. Sci., Polym. Phys. Ed.* **1985**, *23*, 159.
(27) Colby, R. H.; Rubinstein, M. *Macromolecules* **1990**, *23*, 2753.
(28) Daniels, D. R.; McLeish, T. C. B.; Kant, R.; Crosby, B. J.; Young, R. N.; Pryke, A.; Allgaier, J.; Groves, D. J.; Hawkins, R. J. *Rheol. Acta* **2001**, *40*, 403. Raju, V. R.; Menezes, E. V.; Marin, G.; Graessley, W. W. *Macromolecules* **1981**, *14*, 1668. Tao, H.; Huang, C.; Lodge, T. P. *Macromolecules* **1999**, *32*, 1212.
(29) Frischknecht, A. L.; Milner, S. T.; Pryke, A.; Young, R. N.; Hawkins, R.; McLeish, T. C. B. *Macromolecules* **2002**, *35*, 4801.
(30) Miros, A.; Vlassopoulos, D.; Likthman, A. E.; Roovers, J. *J. Rheol.* **2003**, *47*, 163.
(31) McLeish, T. C. B.; Larson, R. G. *J. Rheol.* **1998**, *42*, 81.
(32) Frischknecht, A. L.; Milner, S. T. *Macromolecules* **2000**, *33*, 9764.
(33) Kapnistos, M.; Semenov, A. N.; Vlassopoulos, D.; Roovers, J. *J. Chem. Phys.* **1999**, *111*, 1753.
(34) Larson, R. G.; Sridhar, T.; Leal, L. G.; McKinley, G. H.; Likhtman, A. E.; McLeish, T. C. B. *J. Rheol.* **2003**, *47*, 809.
(35) Juliani; Archer, L. A. *Macromolecules* **2002**, *35*, 10048.
(36) Note, however, that the high-frequency model prediction is expected to be less accurate because the data in that region are also influenced by the segmental relaxation, which is not accounted for theoretically.
(37) Wang, S.; Wang, S.-Q.; Halasa, A.; Hsu, W.-L. *Macromolecules* **2003**, *36*, 5355.

(38) Park, S. J.; Larson, R. G. *Macromolecules* **2004**, *37*, 597. Park, S. J.; Larson, R. G. *J. Rheol.* **2003**, *47*, 199.
(39) Archer, L. A.; Juliani *Macromolecules* **2004**, *37*, 1076.
(40) Viovy, J. L.; Rubinstein, M.; Colby, R. H. *Macromolecules* **1991**, *24*, 3587.
(41) Rubinstein, M.; Colby, R. H. *J. Chem. Phys.* **1988**, *89*, 5291.
(42) des Cloizeaux, J. *Macromolecules* **1990**, *23*, 3992. Tsenoglou, C. *Macromolecules* **1991**, *24*, 1762. Tuminello, W. H. *Polym. Eng. Sci.* **1986**, *26*, 1339.
(43) Doi, M.; Graessley, W. W.; Helfand, E.; Pearson, D. S. *Macromolecules* **1987**, *20*, 1900.
(44) Watanabe, H.; Ishida, S.; Matsumiya, Y.; Inoue, T. *Macromolecules* **2004**, *37*, 1937. Watanabe, H.; Ishida, S.; Matsumiya, Y.; Inoue, T. *Macromolecules* **2004**, *37*, 6619.
(45) Watanabe, H.; Matsumiya, Y.; Inoue, T. *Macromolecules* **2002**, *35*, 2339.
(46) McLeish, T. C. B. *J. Rheol.* **2003**, *47*, 177.
(47) Vlassopoulos, D.; Fytas, G.; Loppinet, B.; Isel, F.; Lutz, P.; Benoit, H. *Macromolecules* **2000**, *33*, 5960.
(48) Lipson, J. E. G. *Macromolecules* **1993**, *26*, 203. Lipson, J. E. G.; Gaunt, D. S.; Wilkinson, M. K.; Whittington, S. G. *Macromolecules* **1987**, *20*, 186.
(49) The small number of branches case is included for completeness. This particular case is considered for a series of starlike combs with few branches per star arm (Kapnistos et al., in preparation).

MA050644X